Step Response of Mouse Rod Photoreceptors Modeled in Terms of Elemental Photic Signals

Gabriel A. Silva and David R. Pepperberg*

***Abstract*—The process of light adaptation in rod photoreceptors enables these sensory cells of the retina to remain responsive to photic stimuli over a broad range of light intensity. Recent studies have employed the technique of paired-flash electroretinography to determine properties of phototransduction, and of light and dark adaptation, in rod photoreceptors in the living eye. Building on these studies, we have developed a theoretical model aimed at explaining the rod electrical response to a step of light based on known physiology. The central feature of the model is its description of the macroscopic (i.e., measured) response in terms of a time-evolving, weighted sum of elemental responses determined under dark-adapted and near fully light-adapted conditions. The model yields a time-dependent function that describes the course of desensitization and putatively represents the cumulative dynamics of underlying biochemical processes involved in light adaptation of the rod.**

***Index Terms*—Electroretinography, light adaptation, physiological modeling, rod photoreceptors.**

I. Introduction

PHOTOCURRENT data obtained from single rod photoreceptors of both lower vertebrates and mammals show that background illumination desensitizes, or "adapts," the phototransduction process in these sensory neurons [1]–[10]. Evidence for this desensitization comes in part from experiments that have compared the rod response to a brief test flash presented under dark-adapted conditions (i.e., in the absence of recent photic stimulation) with the response to the same flash superimposed on a maintained luminous background. For example, background light of moderate intensity shifts, to a higher value, the test flash strength required to half-saturate the prevailing maximal flash response. Determining the mechanisms that underlie background desensitization is a major focus of current research on phototransduction (for reviews, see [11]–[13]).

Manuscript received August 14, 2002; revised April 21, 2003. This work was supported in part by the National Institutes of Health (NIH) under Grant EY-05494 and Grant EY-01792 and in part by an unrestricted grant from Research to Prevent Blindness, Inc. (New York, NY). The work of G. A. Silva was supported in part by a fellowship from the Natural Sciences and Engineering Research Council of Canada (NSERC). *Asterisk indicates corresponding author.*

G. A. Silva was with the Department of Ophthalmology and Visual Sciences, and Department of Bioengineering, University of Illinois at Chicago, College of Medicine, Chicago, IL 60612 USA. He is now with the Departments of Bioengineering and Ophthalmology, University of California at San Diego, La Jolla, CA 92093 USA (e-mail: gsilva@ucsd.edu).

*D. R. Pepperberg is with the Department of Ophthalmology and Visual Sciences, and Department of Bioengineering, University of Illinois at Chicago, College of Medicine, 1855 W. Taylor St., Chicago, IL 60612 USA (e-mail: davipepp@uic.edu).

Digital Object Identifier 10.1109/TBME.2003.820354

The electroretinogram (ERG), a multicomponent signal that can be recorded noninvasively from the intact eye *in vivo*, reflects the massed, light-evoked electrical activities of multiple types of retinal neurons. However, the *in vivo* massed response of the rod photoreceptors themselves can, to a good approximation, be derived computationally using a "paired-flash" ERG technique [14]–[21]. Recently, [22] have employed this technique to examine the effects of background light on the response properties of mouse rod photoreceptors. A central experiment of that study was determination of the ERG-derived rod response to the onset of background illumination, i.e., to a step of light. The results obtained showed that for the steady-state condition that produces a roughly half-saturating response, the derived dynamic rod response to the step of light, that is, the temporal evolution of the rod response toward steady-state, is well described by an analytic function that exhibits an initial rise to peak and a subsequent relaxation, or sag, to the steady-state value within $\sim$1 s after light onset [22]. This step response resembles that observed for rods *in vitro*, and its time course reflects the transition of the rod from dark- to light-adapted state.

Rod phototransduction involves a cascade of biochemical reactions that highly amplify the signal initiated by individual events of visual pigment photoactivation, i.e., by individual photon absorptions. Furthermore, although much remains to be learned about the molecular mechanisms of rod light adaptation, it is clear that this desensitizing process involves modulation of the elemental (i.e., single-photon) response. Thus, the availability of a rod light-adaptation model based on the temporal evolution of single-photon responses may serve as a useful tool in both the interpretation of available experimental data and the design of future experiments. This paper describes the construction and application of such a model.

We begin by deriving a set of "basis functions" from weak flash responses obtained under dark-adapted and maximally light-adapted conditions. Through application of a stochastic error-minimizing algorithm, we then show that the development of the light-adapted state induced by onset of a step of light can be described in terms of intermediate light-adapting responses formed by a time-varying weighted sum of the basis functions. These intermediate responses are determined as a discrete time process, one for which the sampling rate corresponds with the average rate of photon arrival inferred for a particular background. The weighted sum of the basis functions is determined by the model-derived function $\omega(t)$, the key output of the model, which is interpreted to describe the putative dynamics of the lumped biochemistry underlying light adaptation. Preliminary results have been reported in abstract form [23].

II. Derivation of Elemental Responses

It is well established that rods are quantum detectors, in the sense that under fully dark-adapted conditions they generate a measurable response upon absorption of a single photon. Under light-adapted as well as dark-adapted conditions, the macroscopic response recorded from a single rod via electroretinography is the summation of these elemental responses, subject to the saturating nonlinearity of the rod (i.e., closure of a progressively greater fraction of cGMP-gated channels in the outer segment) and feedback/deactivation processes that shape the overall response. Recent experiments employing paired-flash ERG recordings in mouse have determined the derived rod response to a test flash delivered under dark-adapted conditions and in steady background light. This derived response, determined with full field ERG stimuli, is a measure of the massed and, thus, averaged, response of the millions of rod photoreceptors in the retina. Under the range of conditions investigated, the derived flash response is well described by the relationship (see [22, eq. 5])

$$\frac{A(t)}{A_{mo}} = 1 - \exp\left[-I_{\text{test}} \cdot \varepsilon(t)\right];$$
$$\varepsilon(t) = \phi\left\{1 - \exp\left[-\alpha(t - t_d)^2\right]\right\} \exp\left(-\frac{t}{\tau_\omega}\right) \quad (1)$$

where I_{test} is the strength [here in luminance units of scotopic candela s m^{-2}(sc cd s m^{-2})] of a brief stimulating flash; $A(t)$ is the derived response of a typical rod to this test flash (see [18] and [22]), A_{mo} is the prevailing maximal amplitude of the rod response; t_d is a fixed delay; ϕ, α, and τ_ω are fitted parameters; and $\varepsilon(\text{t})$ is a time-dependent function that has units of inverse flash strength $[(\text{sc cd s m}^{-2})^{-1}]$ but is independent of flash strength (i.e., independent of the value of I_{test}).

For purposes of the present model it is useful to introduce the scaling factor η that converts $\varepsilon(t)$ to $\varepsilon_o(t)$, a dimensionless unit response associated with a single photoisomerization (photoactivation of a single molecule of rhodopsin)

$$\varepsilon_0(t) = \eta \cdot \varepsilon(t) \quad (2.1)$$
$$\frac{A(t)}{A_{mo}} = 1 - \exp\left[-I_{\text{test}} \cdot \eta^{-1} \cdot \varepsilon_0(t)\right]. \quad (2.2)$$

Here, the excitatory signal $\varepsilon(t)$ is replaced by the product $(\eta^{-1} \cdot \varepsilon_o(t))$. $\varepsilon(t)$ in (1) and (2.1) displays a time course identical to that of $\varepsilon_o(t)$, but with an amplitude determined by the value of the scaling factor η. We now define $\varepsilon_{\text{oDA}}(t)$, η_{DA} and A_{moD} as the dark-adapted forms of $\varepsilon_o(t)$, η and A_{mo}, respectively. If we further symbolize by Φ the number of photoisomerizations per rod produced by the test flash, η_{DA} will have units of [sc cd s m^{-2}/Φ]. Equating 1 sc cd s m^{-2} with 100 Φ in the dark-adapted mouse eye [18], [22], η_{DA} is equal to 0.010 [sc cd s m^{-2}/Φ]. As noted above, η_{DA} is in essence a scaling factor that transforms $\varepsilon_{\text{DA}}(t)$ into a dimensionless single-photon response, $\varepsilon_{\text{oDA}}(t)$. Curve 1 in Fig. 1(a) illustrates $\varepsilon_{\text{oDA}}(t)$ normalized to its peak amplitude. Thus, given a flash strength Φ, where the physical units of Φ are photoisomerizations per rod, the macroscopic derived response $A(t)/A_{moD}$ is related to the single-photon dark-adapted response $\varepsilon_{\text{oDA}}(t)$ by

$$\frac{A(t)}{A_{moD}} = 1 - \exp\left[-\Phi \cdot \varepsilon_{\text{oDA}}(t)\right]. \quad (3)$$

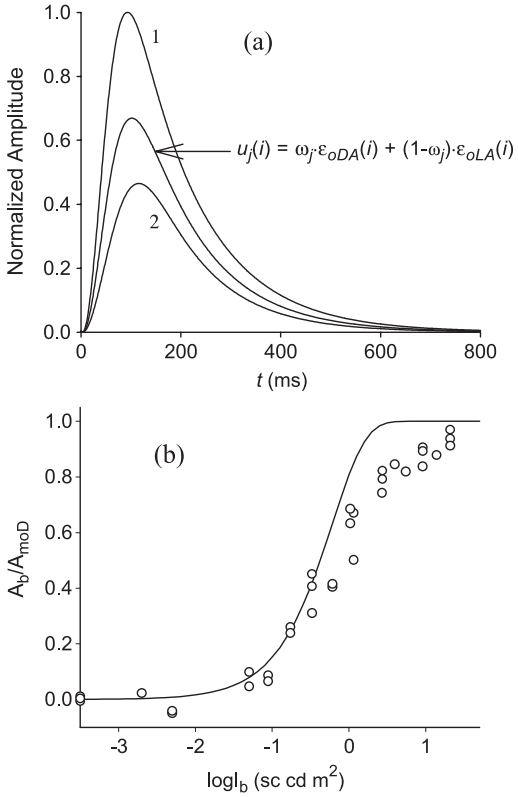

Fig. 1. Modeling intermediate elemental responses. (a) Representative intermediate elemental response $u_j(i)$ generated during light adaptation. $u_j(i)$ is the weighted sum of the dark-adapted ($\varepsilon_{\text{oDA}}(t)$; curve 1) and maximally light-adapted ($\varepsilon_{\text{oLA}}(t)$; curve 2) elemental responses, determined by the weighting parameter ω_j, here equal to 0.4. As described in [18] and [22], the functions $\varepsilon_{\text{DA}}(t)$ and $\varepsilon_{\text{LA}}(t)$ leading to the present $\varepsilon_{\text{oDA}}(t)$ and $\varepsilon_{oLA}(t)$ are based on experimental data obtained under dark-adapted conditions (for $\varepsilon_{\text{DA}}(t)$) and with a 1.2 sc cd m^{-2} background (for $\varepsilon_{\text{oLA}}(t)$; test flash of 0.98 sc cd s m^{-2}). (b) Normalized amplitude A_b/A_{moD} of the derived rod response to steady background light, plotted against the logarithm of background strength ($\log I_b$). Data obtained in paired-flash ERG experiments on mice. Solid curve: plot of the relation $\text{A}_b/\text{A}_{moD} = 1 - \exp(-\text{k}_{86}\, I_b\, \tau_{\text{int}})$ (see [22, eq. 4]). The integration time τ_{int} is defined by $[\text{A}(86)/\text{A}_{moD}] \cdot \tau_{\text{int}} = \int[\text{A}(t)/\text{A}_{\text{moD}}]\text{d}t$, where $\text{A}(t)/\text{A}_{moD}$ is the normalized dark-adapted response to a 0.12 sc cd s m^{-2} test flash (see [18, eq. 6]), and where $\text{A}(86)/\text{A}_{moD}$ is the normalized amplitude at $t = 86$ ms. The integration was carried out over the range $0 \leq t \leq 1000$ ms, yielding $\tau_{\text{int}} = 235$ ms. (b) Adapted from [22] with permission of The Physiological Society.

We now consider a counterpart elemental response associated with the near fully or maximally light-adapted state that develops upon the step onset of relatively strong background light. We furthermore define, by A_b, the rod response maintained in continuous background light of this intensity. In the absence of light adaptation, the maintained normalized response A_b/A_{moD} would be expected to reflect the summed action of continuously generated, dark-adapted single-photon responses $\varepsilon_{\text{oDA}}(t)$. The need for derivation of a steady-state, maximally light-adapted elemental response, $\varepsilon_{oLA}(t)$, is based on the experimental observation that with increasing background intensity, the dark-adapted response based on $\varepsilon_{\text{oDA}}(t)$ becomes a progressively poorer approximation to the observed response. Fig. 1(b) illustrates this effect in relation to the integration time determined for the dark-adapted response $\varepsilon_{\text{DA}}(t)$. As illustrated by the curve, the background dependence of maintained amplitude predicted with an unchanging integration time accounts well for the observed amplitudes at weaker backgrounds, but underestimates

the desensitization produced by brighter backgrounds. That is, the dependence of maintained amplitude is more gradual than that predicted by the adaptation-free curve (see [18] and [22]). [22] determined derived flash responses in background light and analyzed those data in terms of light-adapted elemental functions (see [22, eq. 4]). Here, we represent the maintained background response A_b/A_{moD} and the light-adapted flash response $A(t)/A_{moD}$ in forms parallel to those of (2) and (3)

$$\frac{A_b}{A_{moD}} = 1 - \exp\left[-I_b \cdot \int_{l=0}^{\infty} \varepsilon_{\mathrm{LA}}(t, I_b)dt\right] \tag{4.1}$$

$$\frac{A(t)}{A_{moD}} = 1 - \exp\left[-I_{\mathrm{test}} \cdot \eta_{\mathrm{LA}}^{-1} \cdot \varepsilon_{\mathrm{oLA}}(t)\right] \tag{4.2}$$

$$\frac{A_b}{A_{moD}} = 1 - \exp\left[-\nu \cdot \int_{0}^{\infty} \varepsilon_{\mathrm{oLA}}(t)dt\right] \tag{4.3}$$

where I_b is in units of sc cd m^{-2} and $\varepsilon_{\mathrm{LA}}(t, I_b)$ is the response function defined earlier for varying backgrounds I_b. As in the dark-adapted case, we can express $\varepsilon_{\mathrm{LA}}(t)$ as the product of a presumed single-photon light-adapted response $\varepsilon_{\mathrm{o}LA}(t)$ and a scaling factor η_{LA} (4.2). Equation (4.3) rewrites (4.1) in terms of ν, a variable that represents the average frequency of photon arrival and that has physical units of photoisomerizations per rod per second. Although photon arrival is a stochastic process, the average frequency of photoisomerizations is simply determined by the background strength (in photoisomerizations rod^{-1} s^{-1}).

Although both $\varepsilon_{\mathrm{oLA}}(t)$ and $\varepsilon_{\mathrm{LA}}(t)$ are functionally similar to their dark-adapted counterparts, both functions depend on background strength as well as time (i.e., $\varepsilon_{\mathrm{LA}}(t, I_b)$ and $\varepsilon_{\mathrm{oLA}}(t, I_b)$) (see [22]). However, experimental data indicate that the normalized sensitivity of the rod reaches a near-fully light-adapted state in background light of strength 1.2 sc cd m^{-2} (cf. [22, Figs. 3 and 4, Table 1, and Discussion]). On this basis, we henceforth interpret the elemental function determined for the background condition of 1.2 sc cd m^{-2} as a fully light-adapted single-photon response. The value of η_{LA} relevant to this condition can be determined by considering that the step response to a 1.2 sc cd m^{-2} background has a steady-state amplitude equal to 0.54 (see [22, Fig. 4]). Therefore, using (4.1)–(4.3), $0.54 = 1 - \exp[-I_b \cdot \int_0^{\infty} \varepsilon_{\mathrm{LA}}(t)dt]$. With $I_b = 1.2$ sc cd m^{-2}, the exponent of the preceding expression is $0.78 = [-I_b \cdot \int_{t=0}^{\infty} \varepsilon_{\mathrm{LA}}(t)dt] = [-\nu \cdot \int_0^{\infty} \varepsilon_{\mathrm{oLA}}(t)dt] = [-\nu \cdot \eta_{\mathrm{LA}} \cdot \int_0^{\infty} \varepsilon_{\mathrm{LA}}(t)dt]$, where $\nu = 120$ photoisomerizations rod^{-1}s^{-1}. The integrated area of $\varepsilon_{\mathrm{LA}}(t)$ at 1.2 sc cd m^{-2} from 0 to 1000 ms is 0.30 [(sc cd s m^{-2})$^{-1}$ms] which yields $\eta_{\mathrm{LA}} = 0.0217$ sc cd s m$^{-2}/\Phi$. Curve 2 in Fig. 1(a) shows $\varepsilon_{\mathrm{oLA}}(t)$ for $I_b = 1.2$ sc cd m^{-2}. In the following sections, we use (3) and (4) to model the step response to a background of a defined photon frequency.

III. Model Construction

A. Conceptual and Mathematical Model Structure

We now use $\varepsilon_{\mathrm{oDA}}(t)$ and $\varepsilon_{\mathrm{oLA}}(t)$ as basis functions to model the time-evolution of the single-photon signal and the corresponding macroscopic experimentally derived response to the stepped onset of background light. Qualitatively, the model describes how during the period over which the rods light-adapt to the background (about 1 s for mouse rods exposed to weak or moderate backgrounds [22]), intermediate responses generated by progressively later arriving photons display greater degrees of desensitization. This desensitization, manifested as progressively decreased peak amplitudes and faster falling-phase kinetics of the intermediate rersponses, continues until attainment of the steady-state condition is achieved, at which time subsequent responses display no further changes to the maintained background and are by definition fully adapted to that background.

Fig. 1(a) illustrates how a hypothetical intermediate light-adapted response, $u_j(i)$, is generated following the step onset of a background, as the weighted summation of the elemental responses $\varepsilon_{\mathrm{oDA}}(t)$ and $\varepsilon_{\mathrm{oLA}}(t)$. For a discrete time process sampled at the period of photon arrival, each intermediate response $u_j(i)$ can be described as a weighted sum of $\varepsilon_{\mathrm{oDA}}(i)$ and $\varepsilon_{\mathrm{oLA}}(i)$ by

$$u_j(i) = \omega_j \varepsilon_{\mathrm{oDA}}(i) + (1 - \omega_j)\varepsilon_{\mathrm{oLA}}(i). \tag{5}$$

The weighting parameter $\omega_j (0 \leq \omega_j \leq 1)$ determines the peak amplitude and shape of $u_j(i)$ by determining the degree of contribution from $\varepsilon_{\mathrm{oDA}}(t)$ and $\varepsilon_{\mathrm{oLA}}(t)$. When the background of fixed strength is turned on, a stream of photons arrives at the rod at a fixed average frequency. The intermediate response $u_j(i)$ is generated by the jth arriving photon, and its amplitude sampled at discrete intervals defined by i, such that $i = 0$ is defined uniquely for each intermediate response at the moment it begins. Both indexes i and j are $\in \{1, 2, 3, \ldots, N\}$, such that discrete time sampling occurs at $i \cdot P$ and $j \cdot P$, where P is defined as the period that separates the arrival of consecutive photons (i.e., the inverse of the average frequency ν, see above). Each intermediate response is uniquely labeled as a function of the photon that produces it, identified by the subscript j. Implicit in this construction is a central assumption of the model: namely, once an intermediate response is initiated by an arriving photon and its dynamics determined by ω_j, it evolves independent of the generation of any previous or subsequent responses (see, also, Fig. 2). This is taken into account in (5) by the fact that the time index i is independent of the absolute time at which the intermediate response is generated (i.e., for all j, $i = [0, 1, 2, \ldots]$), and is governed only by the kinetics of $\varepsilon_{\mathrm{oDA}}(t)$ and $\varepsilon_{\mathrm{oLA}}(t, I_b)$ weighted to ω_j. This assumption is based on experimental results which suggest that molecular events early in the evolution of the elemental response govern the time course of rhodopsin's activity [24]–[29]. In the example of Fig. 1(a) $u_j(i)$ was produced using (5) with $\omega_j = 0.40$. It is the set of parameters ω_j that describes the temporal dynamics of the adaptation process, since it is these parameters that determine how intermediate responses evolve from dark- to light-adapted character.

Fig. 2 illustrates the first three intermediate elemental responses produced by a background step initiated at $j = 0$. Curve $u_1(i)$ in Fig. 2 is the response to the first photon in a train of arriving photons following background onset, thus, $u_1(i)$ is identical to $\varepsilon_{\mathrm{oDA}}(t)$. Curves $u_2(i)$ and $u_3(i)$ in Fig. 2 show the next two hypothetical intermediate responses produced by subsequently arriving photons, each produced by weighted sums

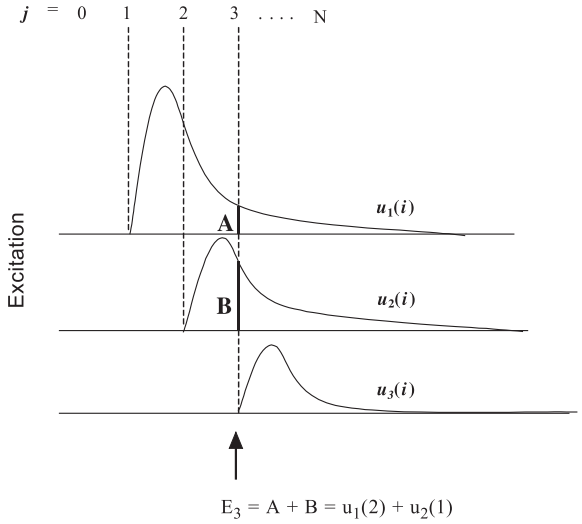

Fig. 2. The amplitudes of intermediate light-adapting responses $u_j(i)$ summate at times j, equal to the times of photon arrival at the rod photoreceptor, to theoretically yield the fractional excitation amplitude E_j. The array of excitation amplitudes E_j and the continuous time function fitted to them, $E(t)$, can be derived from the experimentally determined rod step response function [cf. (7), see text].

of $\varepsilon_{\mathrm{oDA}}(t)$ and $\varepsilon_{\mathrm{oLA}}(t)$. Note in Fig. 2 and in the description just given, that each intermediate response is in a slightly different stage of light adaptation. At any fixed time j after background onset and before the full development of adaptation, different intermediate responses will contribute differing amplitudes. This occurs because responses initiated at different times after background onset have a lifetime much longer than the period between photon arrival events (and, hence, generation of new responses), ensuring overlap of responses that are in different stages of their evolution. For example, a half-saturating 1.2 sc cd m^{-2} background produces roughly 120 photoisomerizations rod^{-1} s^{-1}, or on average one photon every 8.2 ms, each resulting in an intermediate response. But as evident from Fig. 1(a), responses last more than 500 ms [cf. (1) and (2)], causing a considerable overlap between responses. Different intermediate responses will furthermore have slightly different peak amplitudes and kinetics, since each subsequent response is slightly more light-adapted then the previous one. The result of this relationship is that, at any given time j, the shape of a given intermediate response will differ from all others present at that instant.

The sum of all overlapping amplitudes from intermediate responses $u_j(i)$ at a specific index j can be considered to yield an amplitude E_j, such that, as a function of time

$$E_j = \sum_{k=1}^{j-1} u_k(j-k) = \sum_{k=1}^{j-1} \left[\omega_k \varepsilon_{\mathrm{oDA}}(j-k) + (1-\omega_k)\varepsilon_{\mathrm{oLA}}(j-k)\right]. \quad (6)$$

E_j represents the amount of fractional excitation or amplitude contributed by all overlapping intermediate responses at a given time j. E_j can be derived from the experimentally determined step response function via the transformation

$$\frac{A(t)}{A_{moD}} = 1 - \exp\left[-\eta_o \cdot E(t)\right] \quad (7)$$

where η_o is a factor that scales $E(t)$, the continuous time counterpart of E_j. It should be noted that there is no need to numerically determine the scaling factor η_o, since it is implicitly taken into account by η_{DA} and η_{LA} (see Appendix). Furthermore, η_o is a time independent scaling factor. The excitation function Ej is the link between the experimentally determined step response and the single-photon intermediate responses, which are themselves constructed as the weighted sum of dark- and maximally desensitized light-adapted elemental responses, $\varepsilon_{\mathrm{oDA}}(t)$ and $\varepsilon_{\mathrm{oLA}}(t)$. The critical set of weighting parameters ω_j is determined from the experimentally derived step response functions through (7).

B. Model Convergence by the Recursive Stochastic Algorithm

Equation (5) employs the set of parameters ω_j to represent the dynamics of the background step response. We now show how to determine the ω_j parameters that yield the best-fit model response functions to experimentally derived step responses for different backgrounds. Determination of the ω_j parameters is achieved by the convergence of a recursive stochastic error-minimizing algorithm described in detail below. We begin by choosing a general function for $\omega(t)$, the time-continuous function consisting of the collection of parameter values ω_j, which satisfies several requirements implied by the known physiology. First, since desensitization is a delayed process for weak to moderate backgrounds, the functional form of $\omega(t)$ at times shortly after time zero should be near unity (i.e., yielding intermediate responses similar to $\varepsilon_{\mathrm{oDA}}(t)$). Second, with attainment of the steady-state, the mix of $\varepsilon_{\mathrm{oDA}}(t)$ and $\varepsilon_{\mathrm{oLA}}(t)$, and thus, the plateau value of $\omega(t)$, will be some value $0 \leq \omega(t)\,\mathrm{plateau} \leq 1$. A relatively simple mathematical expression that satisfies these constraints is a function of the form

$$\omega(t) = \frac{\left[1 + c_1 \cdot \exp\left\{c_2 \cdot (t - c_3)\right\}\right]}{\left[1 + \exp\left\{c_2 \cdot (t - c_3)\right\}\right]} \quad (8)$$

that contains three free parameters to be fitted. Here, the parameter c_1 is dimensionless, c_2 has units of inverse time, and c_3 has units of time. This selected form of $\omega(t)$ is not derived from the kinetics of a known physiological or biochemical process. Rather, the form of (8) was chosen as a relatively simple function that has the potential to exhibit near unit value at $t = 0$ and following a delay can decline smoothly toward an asymptotic value between zero and unity. This function is sampled at intervals $j \cdot P$ (where the index j and the period of photon arrival P are as defined earlier), which define the set of parameters ω_j used to calculate the model-derived step response $E(t)$. Note that throughout the remainder of this paper, the algebraic form of $\omega(t)$ remains that shown in (8), but with different numerical evaluations of its parameters.

The recursive stochastic algorithm that determines $E(t)$ is a modification of the classical statistical training algorithm used to train the weights of back-propagating neural networks (see

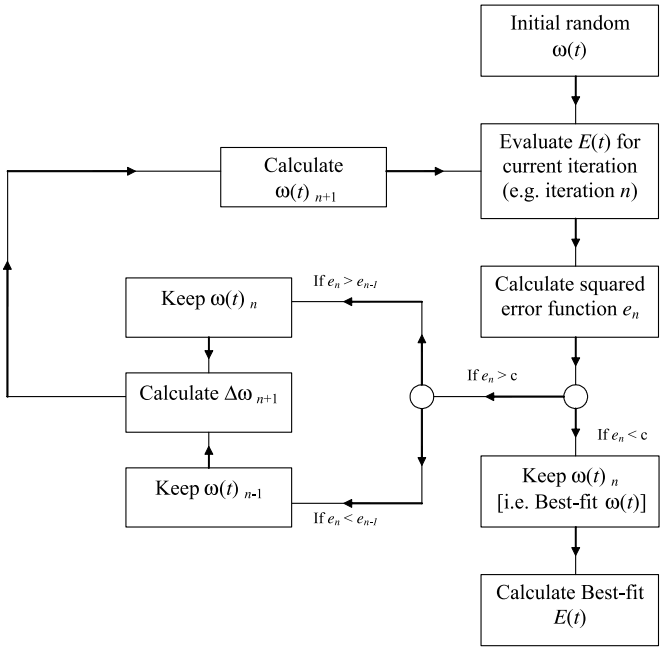

Fig. 3. Flow diagram illustrating the key steps in the operation of the recursive stochastic algorithm (see Appendix for details).

[30]). Fig. 3 illustrates a flow diagram of the key steps in its operation. In particular, the box labeled "Evaluate $E(t)$ for current iteration" is the key step that takes the set of ω_j parameters and calculates the resulting $E(t)$ using (5) and (6). When applied to experimental data, the model determines an $\omega(t)$ function that produces a model-derived best-fit step response function as described earlier via a statistical optimization routine that minimizes an error function. Through a series of iterations, the model converges toward a best-fit solution for $E(t)$ within an arbitrarily small error (Appendix).

IV. Model Simulations

The model can be tested and its operation illustrated by evaluating the resulting step response $E(t)$ given an $\omega(t)$ function with prespecified numerical values of the parameters c_1, c_2, and c_3 for the algebraic form of $\omega(t)$ given in (8). Fig. 4(a) illustrates four cases where the asymptotic value of $\omega(t)$ was set at 0.1, 0.2, 0.4, and 0.9. Here, as well as in all subsequent sections, implementation of the model was done using Matlab (Mathworks Inc., Natick MA). Results of these simulations for backgrounds of 1.2 and 0.4 $\mathrm{sc\ cd\ m^{-2}}$ (i.e., sampling periods of 8.3 and 25 ms, respectively) are shown in Fig. 4(b)–(e) generated by curves 1–4 in Fig. 4(a), respectively. All step response curves were evaluated for N data points assuming a sampling period T, where in each case the product $N \cdot T$ was fixed at 900 ms. Qualitatively, the behavior of the resulting step response functions obtained with curves 1–4 in Fig. 4(a) was similar to that of the experimental data. Note that the 1.2 $\mathrm{sc\ cd\ m^{-2}}$ curve in Fig. 4(e) [generated by curve 4 in Fig. 4(a)] displays an overshoot similar to that seen experimentally.

V. Application to Experimental Data

A. 1.2 sc cd m^{-2} Background

We now apply the stochastic model to experimentally derived step response functions. Fig. 5 illustrates the result of a representative run for a background of intensity 1.2 sc cd $\mathrm{m^{-2}}$. Curve 2 in Fig. 5(a) shows the resulting numerical evaluation of the $\omega(t)$ function [see (8)] that the model converged to in this particular run, which yielded parameter values of $c_1 = 0.0018$, $c_2 = 0.081\ (\mathrm{ms})^{-1}$, and $c_3 = 196$ ms. In general, model-derived $\omega(t)$ functions obtained from different runs display half-rising values and asymptote values that are within 10% of each other (e.g., compare with Fig. 6). Solid curve 2 in Fig. 5(b) illustrates the model-derived best-fit step response function for this run generated by its $\omega(t)$ function [curve 2 in Fig. 5(a), final squared error equal to 0.1035 in this case]. Curve 2 in Fig. 5(b) exhibits a close fit to the experimentally derived step response data and fitted curve (dashed-curve in Fig. 5(b) [22, Fig. 7]). Fig. 5(c) shows a plot of the squared error as a function of iteration for this particular run. The algorithm converges quickly and efficiently toward the best-fit solution.

Fig. 6 illustrates three additional independent runs of the model for the 1.2 $\mathrm{sc\ cd\ m^{-2}}$ step response data. As described in the Appendix, the initial starting parameters for $\omega(t)$ were randomly selected (curves labeled "Initial(random)" in Fig. 6 (a), (c), and (e)]. In each pair of adjacent panels [Fig. 6(a)-(b), (c)-(d), and (e)-(f)], the left-hand panel illustrates the numerical representations of $\omega(t)$ at different iterations as $\omega(t)$ is randomly modified by the stochastic algorithm in an attempt to yield a convergence of the best-fit-algorithm-derived step response (solid curves) to the experimentally derived step response [dashed curve in Fig. 6(b), (d), and (f)]. Intermediate curves, those that occurred as the algorithm attempted to fit different parametric functions, are shown for iteration 30. Different runs required a different number of iterations to converge to an acceptable error level (set to < 0.11 for all of the data presented here) and converged by different routes to their final solution, as is evident in Fig. 6. However, despite the different starting points and paths taken toward final convergence, the best-fit $\omega(t)$ curves are very similar. That is, the model yields best-fit algorithm-derived step response functions (curves labeled "Best fit" in Fig. 6 (b), (d), and (f)] that are statistically identical [i.e., well within the standard deviation of the experimental data, see Fig. 5(b)] to the experimentally derived step response [compare best-fit curves and dashed curves in each of Fig. 6 (b), (d), and (f)].

B. Effect of Altering $\omega(t)$

It is of interest to explore how the best-fit step response function in Fig. 5(b) (curve 2) changes as the corresponding numerical representation of $\omega(t)$ is changed [curve 2 in Fig. 5(a)]. Curves 1 and 3 in Fig. 5(a) illustrate two additional $\omega(t)$ functions that are arbitrary perturbations of the nominal best-fit $\omega(t)$ determined by the algorithm (curve 2). These two curves are similar to curve 2 (parameters c_1 and c_2 unchanged), but have been shifted horizontally by an arbitrary amount by changing

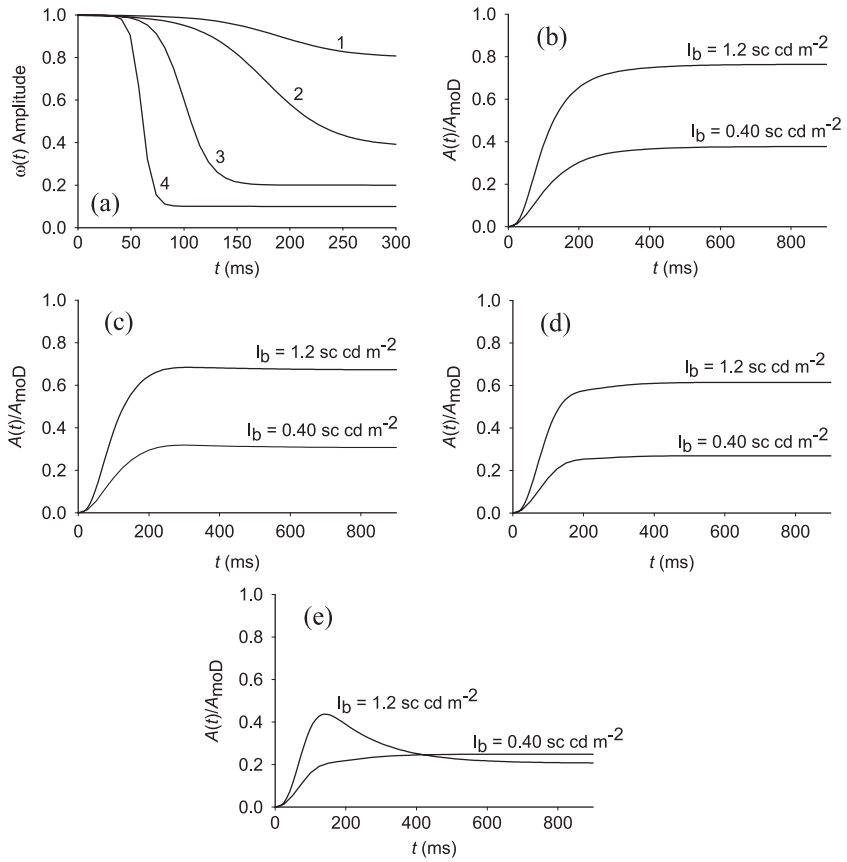

Fig. 4. Generation of simulated weighting functions $\omega(t)$ and determination of corresponding step response functions. (a) Simulated $\omega(t)$ functions given by $\omega(t) = [1 + c_1 \cdot \exp\{c_2(t - c_3)\}]/[1 + \exp\{c_2 \cdot (t - c_3)\}]$, with $c_1 = 0.80$, $c_2 = 0.03$ (ms)$^{-1}$, and $c_3 = 190$ ms (curve 1); $c_1 = 0.40$, $c_2 = 0.030$ (ms)$^{-1}$, and $c_3 = 177$ ms (curve 2); $c_1 = 0.20$, $c_2 = 0.080$ (ms)$^{-1}$, and $c_3 = 100$ ms (curve 3); and $c_1 = 0.10$, $c_2 = 0.20$ (ms)$^{-1}$, and $c_3 = 70$ ms (curve 4). (b)–(e) Simulated step response functions generated from the $\omega(t)$ functions in (a) (curves 1–4 correspond with (b)–(e), respectively). Each panel illustrates simulated step response functions obtained with theoretical background intensities of 0.40 and 1.2 sc cd m^{-2}.

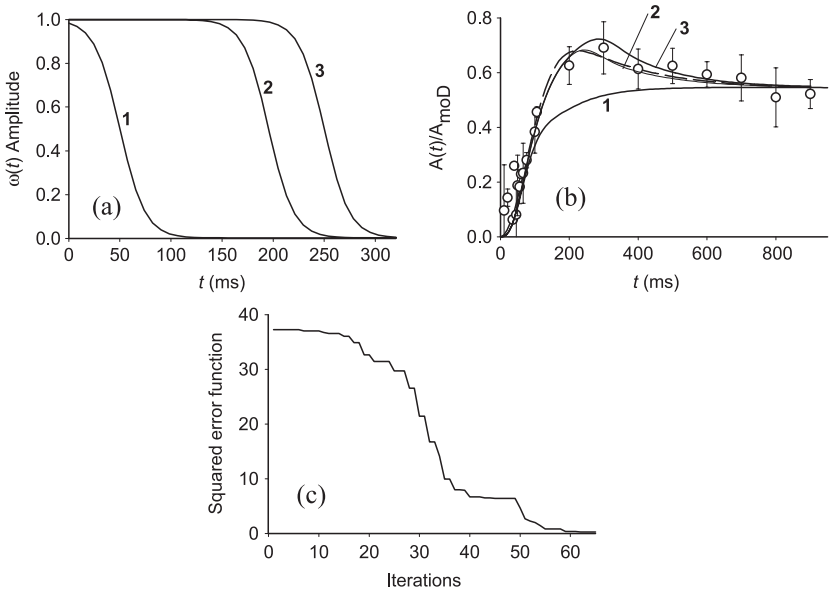

Fig. 5. Representative result obtained with application of the statistical recursive algorithm to the experimentally derived 1.2 sc cd m^{-2} step response. Curve 2 in (a) represents the algorithm-derived weighting function $\omega(t)$ that yielded the best-fit step response function in (b) (curve 2; final convergence yielded a squared error < 0.11). Curves 1 and 3 in (a) are $\omega(t)$ functions similar to curve 2, but arbitrarily shifted along the time axis. The step response functions corresponding with these shifted curves are plotted in (b) as curves 1 and 3, respectively. The open circles in (b) show experimental data obtained with a background step of 1.2 sc cd m^{-2}. The dashed curve is the fit of the empirical equation $(A(t)/A_{moD}) = \{1 - \exp[-\theta(t - t_d)^2]\} \cdot [a_1 + (1 - a_1) \cdot \exp(-t/\tau)]$ [22, Fig. 7] to the data, where $t_d = 3.1$ s and where θ, a_1, and τ are fitted parameters. (c) As a function of the number of iterations, the squared error function associated with the run of the model that yielded curves 2 in (a) and (b). Experimental data and dashed curve in (b) reproduced from [22] with permission of The Physiological Society.

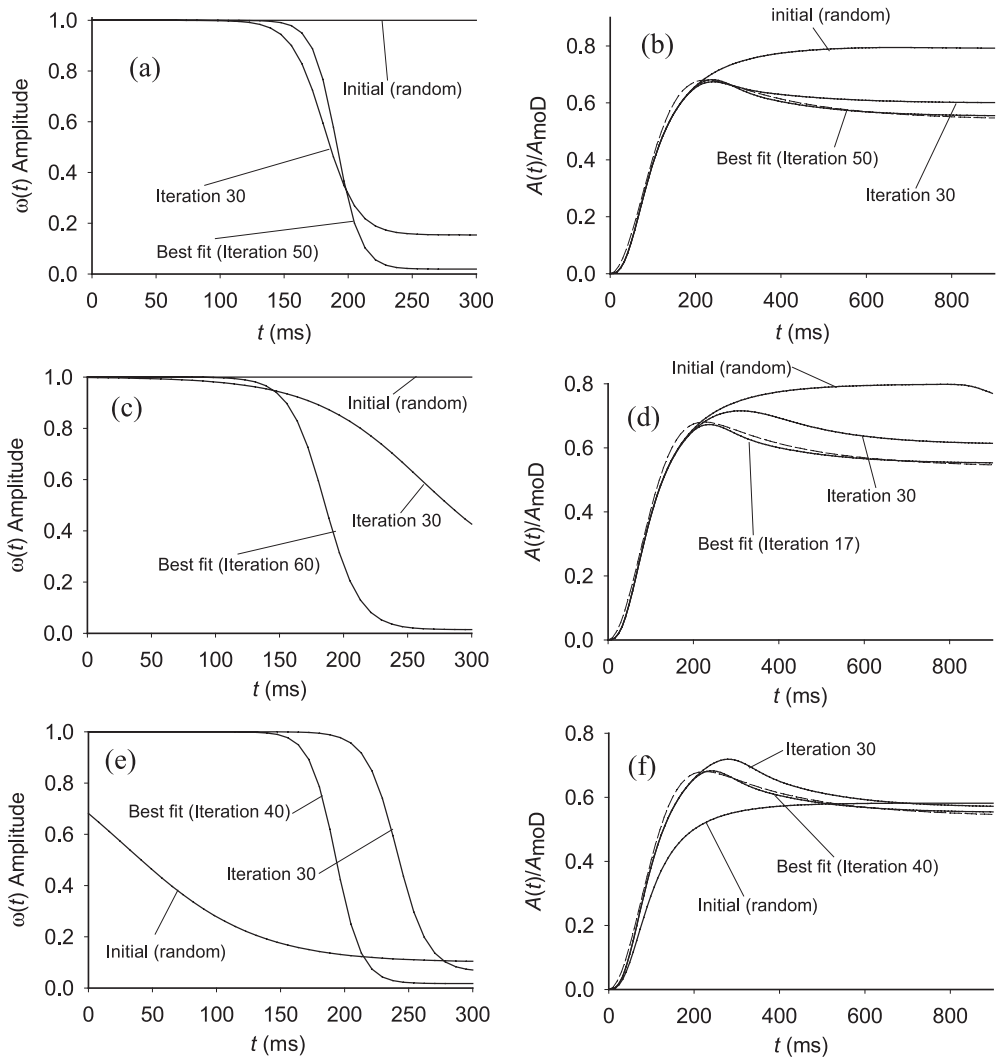

Fig. 6. Application of the recursive statistical algorithm to the experimentally derived 1.2 sc cd m^{-2} step response function. Each pair of adjacent panels corresponds to an independent run of the algorithm. The first panel in each pair [(a), (c), and (e)] illustrates $\omega(t)$ as it is modified based on the degree of convergence of the algorithm-derived best-fit step response [labeled curves in (b), (d), and (f)] with the experimentally derived step response [dashed curve in each of (b), (d), and (f)]. In each case, the starting $\omega(t)$ function is randomly chosen as described in Appendix [curves labeled Initial(random)]. Intermediate curves (at iteration 30), those that occur as the algorithm attempts to fit different parametric functions, are labeled Iteration 30. Curves labeled Best-fit correspond to algorithm best-fit functions.

the value of parameter c_3 ($c_3 = 50$ ms for curve 1, and 250 ms for curve 3). Curves 1 and 3 in Fig. 5(b) are the resulting step response functions evaluated using curves 1 and 3 from Fig. 5(a), respectively. Curves 1 and 3 in Fig. 5(b) do not fit the experimentally derived step response function (dashed curve) as well as curve 2. A rough quantitative measure of the fit of these curves to the experimentally derived step response can be calculated by the root mean square (rms). The rms for curve 2, the model's best-fit step response, measured against the experimentally derived step-response function is 0.0405, while the rms for curves 1 and 3 are 0.1177 and 0.575, respectively. The fit of these curves to the experimental data is more variable due to the scatter in the data themselves. The rms for the experimentally derived step response function (dashed curve) is 0.0836 (see [22]), while the rms for curve 1 is 0.114, for curve 2 is 0.0811, and for curve 3 is 0.0806. Further deviations of $\omega(t)$ from the model derived best-fit $\omega(t)$ produce step response functions with progressively worse fits to both the experimentally determined data and fitted step response curve. For example, keeping the parameters c_1 and c_2 from curve 2 in Fig. 5(a) again unchanged, but altering c_3 from the nominal value of 196 ms to 10 and 350 ms yields rms values 0.1465 and 0.0915, respectively, for the fit to experimental data (curves not shown). Thus, there appears to be a relatively narrow range of $\omega(t)$ functions which yield step response curves that closely approximate the experimentally determined 1.2 sc cd m^2 step response data and fitted function.

C. 0.40 sc cd m^{-2} Background

Fig. 7 illustrates application of the model to experimental data [data points and empirically fitted dashed curve in Fig. 7(a)] determined with a weaker background (0.40 sc cd m^{-2}). The solid curve in Fig. 7(a) is the best-fit algorithm-derived step response function for these data, obtained as described earlier for the 1.2 sc cd m^{-2} data. Fig. 7(b) shows the numerical representation of the $\omega(t)$ function that yielded the solid curve in

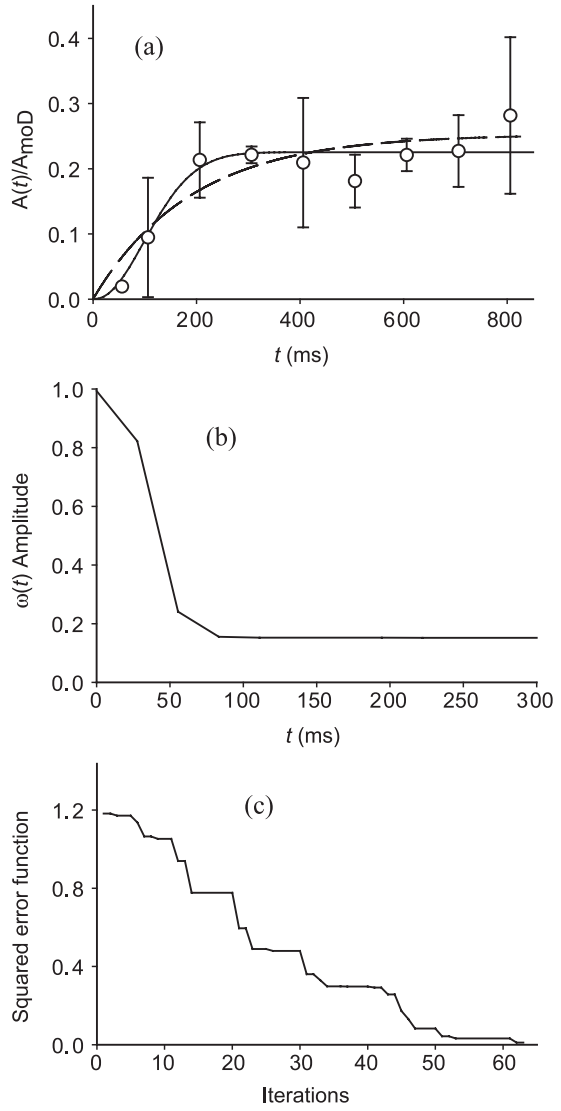

Fig. 7. Representative result obtained with application of the statistical recursive algorithm to experimentally determined 0.40 sc cd m^{-2} step response data. Open circles in (a) show the experimental data obtained with a step background of 0.40 sc cd m^{-2}. The dashed curve is the fit of the empirical equation $A(t)/A_{moD} = d_1[1-\exp(-d_2\, t)]$ to the data, where d_1 and d_2 are fitted parameters [22, Fig. 7]. The solid curve represents the algorithm-derived best-fit step response function; the final convergence yielded a squared error < 0.01. The $\omega(t)$ function in (b) is the algorithm-derived, best-fit weighting function that produced the step response function in (a) (solid curve). (c) Squared error function in relation to the number of iterations. Experimental data and dashed curve in (a) reproduced from [22] with permission of The Physiological Society.

Fig. 7(a). Fig. 7(c) shows the squared error as a function of iteration, and indicates convergence of the model as applied to the 0.40 sc cd m^{-2} data. The coarseness of the resulting algorithm-derived functions is due to the relatively large sampling period ($P = 25$ ms). The kinetics of the resulting best-fit $\omega(t)$ functions tend to be somewhat faster than those of the experimental data obtained with the 1.2 sc cd m^{-2} background, and these functions exhibit a nonzero asymptote (i.e., approximately 0.2) with increasing time. This is consistent with the notion that with this relatively weak background, the steady-state maintained response is not fully light-adapted and, therefore, $\omega(t)$ displays a nonzero asymptote (see above). Together, the results obtained with the 1.2 and the 0.4 sc cd m^{-2} backgrounds indicate that the model converges well to functions consistent with experimental observation.

VI. Discussion

A number of previous studies have investigated, through quantitative modeling, the nature and interplay of the multiple processes involved in phototransduction and light adaptation in rod and cone photoreceptors (e.g., [31]–[37]). In the present study we have modeled the kinetics of the of rod photoreceptor response to a stepped background of defined strength in terms of "basis functions" that represent dark-adapted and maximally light-adapted single-photon responses. These basis functions summate in time-dependent weighted fashion to produce intermediate responses whose peak amplitudes and kinetics evolve with time and track the transition of the rod from the dark- to light-adapted state. A principal goal of the model was to identify the weighting function $\omega(t)$. The construction of the model assumes that the dynamics of $\omega(t)$ are responsible for the observed kinetics of the step response and, therefore, ultimately govern how the rod progresses from the dark- to the light-adapted steady-state.

A. Early Determination of the Elemental Response

A central feature of the present model is the assumption that an intermediate elemental response is fully specified at its instant of initiation. Thus, while both the empirically determined dark-adapted and light-adapted elemental responses $\varepsilon_{oDA}(t)$ and $\varepsilon_{oLA}(t)$ reflect the action of downstream and feedback processes in the phototransduction cascade, their contributions to a given intermediate response (i.e., the prevailing values of ω_j and $1-\omega_j$) are taken as constant and are specified at the instant of initiation of a given intermediate response. This assumption most likely provides at best an approximate description of the trajectory (temporal evolution) of the intermediate response, since it is likely that the influence of downstream and feedback reactions on the intermediate response vary in complex fashion with background intensity and with time after background onset. Furthermore, because the present model's basis functions $\varepsilon_{oDA}(t)$ and $\varepsilon_{oLA}(t)$ are derived from data obtained under dark-adapted conditions and with a 1.2 sc cd m^{-2} background, the model is unlikely to account for adaptation processes that cannot be represented as a weighted sum of the basis functions, e.g., processes that speed or slow response kinetics mainly at backgrounds of intermediate strength. (See for example, results shown in [22, Table 1 and Fig. 5], which include data obtained with a 0.63 sc cd m^{-2} background.) However, the notion of an early time specification of the intermediate response is consistent with evidence indicating a major role of early transduction events in shaping the flash response [24]–[29].

B. Relationship Between η_{DA} and η_{LA}

Use of the dimensionless elemental functions $\varepsilon_{oDA}(t)$ and $\varepsilon_{oLA}(t)$ in the present model has involved the determination of the scaling parameters η_{DA} and η_{LA} that link $\varepsilon_{oDA}(t)$ and $\varepsilon_{oLA}(t)$ with the experimentally determined $\varepsilon_{DA}(t)$ and $\varepsilon_{LA}(t)$ from which they were derived. On a simple view of the system being modeled, one would expect η_{LA} to be equal to η_{DA}, since both link the experimentally used luminance value with a unit photoisomerization (i.e., η_{DA} and η_{LA} essentially

represent rod collecting areas) [see (2)]. The present model indicates, however, that the dark- and light-adapted scaling factors η_{DA} and η_{LA} differ by a factor of approximately 2 ($\eta_{\mathrm{LA}}/\eta_{\mathrm{DA}} = 0.022/0.010 = 2.2$). This disparity suggests either a deficiency in the model or the occurrence of some underlying process that in background-dependent fashion alters the relationship between luminance of the test stimulus and the number of photoisomerizations per rod. This disparity could reflect the fact that the range of photocurrent spanned by the experimentally determined response to a superimposed test flash lies above, i.e., is nearer to saturation than, the photocurrent value maintained by the background itself. As emphasized by recent data from amphibian rods [38], rod adaptation to near saturating backgrounds appears to include processes beyond those responsible for the rapid attainment of steady-state during weaker illumination. Thus, for example, incremental excitation by the test flash during the step response might increase adaptation above the level prevailing during the step alone, and this additional adaptation, if occurring on a fast time scale, might produce an underestimate of $\varepsilon_{\mathrm{oLA}}(t)$. It should also be noted that the variables η_{LA} and ν introduced in Section II multiply one another. Thus, an error in assignment of the numerical value of ν for the 1.2 sc cd m^{-2} background (120 photoisomerizations rod^{-1}s^{-1}) would lead to an error in the numerical value of η_{LA} and perhaps underlie the disparity in numerical values of η_{DA} and η_{LA} noted above.

C. Interpretation of the Weighting Function $\omega(t)$

The present model accounts for the macroscopic step response in terms of a time-dependent weighting function $\omega(t)$ that governs the contribution of elemental photic signals. The dependence of the model on $\omega(t)$ suggests that its dynamics may putatively describe the normalized dynamics of the lumped biochemical processes responsible for light adaptation. Physically, the dynamics of rod light adaptation are determined by the underlying biochemistry responsible for the modulation of transduction processes. A factor thought to play a major role in light adaptation is the light-induced decrease in the intracellular concentration of calcium ($\mathrm{Ca}_{\mathrm{i}}^{2+}$) [2], [12], [28], [39]–[45]. The time course of $\omega(t)$ in the present theoretical study is generally similar to the course of $\mathrm{Ca}_{\mathrm{i}}^{2+}$ decline produced by steps of light in frog and gecko rods *in vitro* [43]–[45]. While no claim is made that the present $\omega(t)$ describes the course of step-induced calcium decrease, the ability of the model to describe the experimentally determined step response suggests that $\omega(t)$ can be viewed as a lumped index of the underlying biochemical processes involved in light-adaptation.

VII. Conclusion

The present model provides an account of the rod light-adaptation process in terms of single-photon responses. Furthermore, it employs *in vivo* mammalian ERG data and, thus, offers relatively direct application to the study of both normal physiology and disease processes in the human eye. Understanding human retinal diseases, and the evaluation of photoreceptor function upon drug or gene therapy intervention, may benefit from studies of rod function through theoretical models of the present type.

Appendix

Operation of the algorithm begins with an initial random guess of the $\omega(t)$ parameters chosen from a uniform random distribution, where the parameter values are within the range $0 \le c_1 \le 1$, $0 \le c_2 \le 0.1$, and $0 \le c_3 \le 1000$ (i.e., a uniform random number generator between zero and one multiplied by factors 1, 0.1, and 1000, respectively). Following this initialization of $\omega(t)$, random changes of its parameters, $\Delta\omega$, are produced by $\Delta\omega = \delta \cdot \mathrm{R}$, where R is a random number chosen from a uniform distribution between 0 and 1, and $\delta = 0.02 + (1 - 0.02) \cdot \exp(-temp \cdot 10)$; $temp = 1 - \exp(-\mathrm{iteration} \cdot 0.001)$. This approach produces smaller $\Delta\omega$ as a function of increasing number of iterations (see [30]). For a given iteration, a simulated $E(t)$ curve ($simE$) is calculated from $\varepsilon_{\mathrm{oDA}}(t)$, $\varepsilon_{\mathrm{oLA}}(t)$ and the $\omega(t)$ function for that particular iteration, as described above. $simE$ is then compared with the $E(t)$ function determined from the experimental step response data ($realE$) by means of a squared error function defined by $e = \sum[simE(i) - realE(i)]^2$. If the squared error for a given iteration is less than the error from the previous iteration, the randomly chosen $\omega(t)$ parameters for that iteration are kept; otherwise they are reset to the values from the previous iteration. Final convergence is reached when the squared error reaches an arbitrary small value (0.011 for the 1.2 sc cd m^{-2} step response data, and 0.01 for the 0.40 sc cd m^{-2} step response data). Technically, determination of $E(t)$ from the experimental step response data via (7) yields the quantity $\eta_o \cdot E(t)$, where the scaling factor η_o is strictly speaking an unknown quantity. With η_{DA} and η_{LA} determined above, a direct comparison between $realE$ and $simE$ is achievable. Therefore, the complete formulation of (6) is given by

$$\begin{aligned}\eta_o \cdot E_j &= \sum_{k=1}^{j-1} \sum_{l=j-1}^{1} u_k(l) \\ &= \sum_{k=1}^{j-1} \sum_{l=j-1}^{1} [\omega_k \cdot \eta_{\mathrm{DA}} \cdot \varepsilon_{\mathrm{oDA}}(l) + (1 - \omega_k) \cdot \eta_{\mathrm{LA}} \\ &\qquad \cdot \varepsilon_{\mathrm{oLA}}(l)]\,. \end{aligned} \tag{A.1}$$

Acknowledgment

Much of this material was contained in a thesis submitted by G. A. Silva to the Department of Bioengineering at the University of Illinois at Chicago, in partial fulfillment of the requirements for the Ph.D. degree.

References

[1] D. A. Baylor, T. D. Lamb, and K.-W. Yau, "Responses of retinal rods to single photons," *J. Physiol.*, vol. 288, pp. 613–634, 1979.
[2] G. L. Fain, T. D. Lamb, H. R. Matthews, and R. L. W. Murphy, "Cytoplasmic calcium as the messenger for light adaptation in salamander rods," *J. Physiol.*, vol. 416, pp. 215–243, 1989.
[3] T. Tamura, K. Nakatani, and K.-W. Yau, "Light adaptation in cat retinal rods," *Science*, vol. 245, pp. 755–758, 1989.
[4] M. C. Cornwall, H. Ripps, R. L. Chappell, and G. J. Jones, "Membrane current responses of skate photoreceptors," *J. Gen. Physiol.*, vol. 94, pp. 633–647, 1989.
[5] M. C. Cornwall, A. Fein, and E. F. MacNichol, Jr., "Cellular mechanisms that underlie bleaching and background adaptation," *J. Gen. Physiol.*, vol. 96, pp. 345–372, 1990.
[6] H. R. Matthews, "Incorporation of chelator into guinea-pig rods shows that calcium mediates mammalian photoreceptor light adaptation," *J. Physiol.*, vol. 436, pp. 93–105, 1991.

[7] K. Nakatani, T. Tamura, and K.-W. Yau, "Light adaptation in retinal rods of the rabbit and two other nonprimate mammals," *J. Gen. Physiol.*, vol. 97, pp. 413–435, 1991.
[8] T. W. Kraft, D. M. Schneeweis, and J. L. Schnapf, "Visual transduction in human rod photoreceptors," *J. Physiol.*, vol. 464, pp. 747–765, 1993.
[9] D. M. Schneeweis and J. L. Schnapf, "Photovoltage of rods and cones in the macaque retina," *Science*, vol. 268, pp. 1053–1056, 1995.
[10] D. M. Schneeweis and J. L. Schnapf, "Noise and light adaptation in rods of the macaque monkey," *Visual Neurosci.*, vol. 17, pp. 659–666, 2000.
[11] P. B. Detwiler and M. P. Gray-Keller, "The mechanisms of vertebrate light adaptation: speeded recovery versus slowed activation," *Curr. Opin. Neurobiol.*, vol. 6, pp. 440–444, 1996.
[12] G. L. Fain, H. R. Matthews, M. C. Cornwall, and Y. Koutalos, "Adaptation in vertebrate photoreceptors," *Physiol. Rev.*, vol. 81, pp. 117–151, 2001.
[13] M. E. Burns and D. A. Baylor, "Activation, deactivation, and adaptation in vertebrate photoreceptor cells," *Ann. Rev. Neurosci.*, vol. 24, pp. 779–805, 2001.
[14] D. G. Birch, D. C. Hood, S. Nusinowitz, and D. R. Pepperberg, "Abnormal activation and inactivation mechanisms of rod transduction in patients with autosomal dominant retinitis pigmentosa and the pro-23-his mutation," *Invest. Ophthalmol. Vis. Sci.*, vol. 36, pp. 1603–1614, 1995.
[15] A. L. Lyubarsky and E. N. Pugh Jr., "Recovery phase of the murine rod photoresponse reconstructed from electroretinographic recordings," *J. Neurosci.*, vol. 16, pp. 563–571, 1996.
[16] D. R. Pepperberg, D. G. Birch, K. P. Hofmann, and D. C. Hood, "Recovery kinetics of human rod phototransduction inferred from the two-branched a-wave saturation function," *J. Opt. Soc. Amer. A*, vol. 13, pp. 586–600, 1996.
[17] D. R. Pepperberg, D. G. Birch, and D. C. Hood, "Photoresponses of human rods *in vivo* derived from paired-flash electroretinograms," *Visual Neurosci.*, vol. 14, pp. 73–82, 1997.
[18] J. R. Hetling and D. R. Pepperberg, "Sensitivity and kinetics of mouse rod flash responses determined *in vivo* from paired-flash electroretinograms," *J. Physiol.*, vol. 516, pp. 593–609, 1999.
[19] M. M. Thomas and T. D. Lamb, "Light adaptation and dark adaptation of human rod photoreceptors measured from the a-wave of the electroretinogram," *J. Physiol.*, vol. 518, pp. 479–496, 1999.
[20] J. G. Robson and L. J. Frishman, "Dissecting the dark-adapted electroretinogram," *Doc. Ophthalmol.*, vol. 95, pp. 187–215, 1999.
[21] C. Friedburg, M. M. Thomas, and T. D. Lamb, "Time course of the flash response of dark-and light-adapted human rod photoreceptors derived from the electroretinogram," *J. Physiol.*, vol. 534, pp. 217–242, 2001.
[22] G. A. Silva, J. R. Hetling, and D. R. Pepperberg, "Dynamic and steady-state light adaptation of mouse rod photoreceptors *in vivo*," *J. Physiol.*, vol. 534, pp. 203–216, 2001.
[23] G. A. Silva and D. R. Pepperberg, "Model of light adaptation of mouse rod photoreceptors based on paired-flash and step-plus-probe ERG data," *Invest. Ophthalmol. Vis. Sci.*, vol. 42, S368 (abstract), 2001.
[24] L. Lagnado and D. A. Baylor , "Calcium controls light-triggered formation of catalytically active rhodopsin," *Nature*, vol. 367, pp. 273–277, 1994.
[25] J. Chen, C. L. Makino, N. S. Peachey, D. A. Baylor, and M. I. Simon, "Mechanisms of rhodopsin inactivation *in vivo* as revealed by a COOH-terminal truncation mutant," *Science*, vol. 267, pp. 374–377, 1995.
[26] H. R. Matthews, "Effects of lowered cytoplasmic calcium concentration and light on the responses of salamander rod photoreceptors," *J. Physiol.*, vol. 484, pp. 267–286, 1995.
[27] ——, "Actions of Ca^{2+} on an early stage in phototransduction revealed by the dynamic fall in Ca^{2+} concentration during the bright flash response," *J. Gen. Physiol.*, vol. 109, pp. 141–146, 1997.
[28] M. P. Gray-Keller and P. B. Detwiler, "Ca^{2+} dependence of dark- and light-adapted flash responses in rod photoreceptors," *Neuron*, vol. 17, pp. 323–331, 1996.
[29] D. R. Pepperberg, "Does rod phototransduction involve the delayed transition of activated rhodopsin to a second, more active catalytic state?," *Visual. Neurosci.*, vol. 15, pp. 1067–1078, 1998.
[30] D. Graupe, *Principles of Artificial Neural Networks*. River Edge, NJ: World Scientific, 1997, pp. 171–186.
[31] D. Tranchina, J. Sneyd, and I. D. Cadenas, "Light adaptation in turtle cones. Testing and analysis of a model for phototransduction," *Biophys. J.*, vol. 60, pp. 217–237, 1991.
[32] T. D. Lamb and E. N. Pugh, Jr., "A quantitative account of the activation steps involved in phototransduction in amphibian photoreceptors," *J. Physiol.*, vol. 449, pp. 719–758, 1992.
[33] Y. Koutalos, K. Nakatani, and K.-W. Yau, "The cGMP-phosphodiesterase and its contribution to sensitivity regulation in retinal rods," *J. Gen. Physiol.*, vol. 106, pp. 891–921, 1995.
[34] F. Rieke and D. A. Baylor, "Single-photon detection by rod cells of the retina," *Rev. Mod. Phys.*, vol. 70, pp. 1027–1036, 1998.
[35] P. B. Detwiler, S. Ramanathan, A. Sengupta, and B. I. Shraiman, "Engineering aspects of enzymatic signal transduction: photoreceptors in the retina," *Biophys. J.*, vol. 79, pp. 2801–2817, 2000.
[36] R. D. Hamer, "Computational analysis of vertebrate phototransduction: combined quantitative and qualitative modeling of dark- and light adapted responses in amphibian rods," *Visual Neurosci.*, vol. 17, pp. 679–699, 2000.
[37] S. Nikonov, T. D. Lamb, and E. N. Pugh, Jr., "The role of steady phosphodiesterase activity in the kinetics and sensitivity of the light-adapted salamander rod photoresponse," *J. Gen. Physiol.*, vol. 116, pp. 795–824, 2000.
[38] P. D. Calvert, V. I. Govardovskii, V. Y. Arshavsky, and C. L. Makino, "Two temporal phases of light adaptation in retinal rods," *J. Gen. Physiol.*, vol. 119, pp. 129–145, 2002.
[39] V. Torre, H. R. Matthews, and T. D. Lamb, "Role of calcium in regulating the cyclic GMP cascade of phototransduction in retinal rods," *Proc. Nat. Acad. Sci., U.S.A.*, vol. 83, pp. 7109–7113, 1986.
[40] H. R. Matthews, R. L. W. Murphy, G. L. Fain, and T. D. Lamb, "Photoreceptor light adaptation is mediated by cytoplasmic calcium concentration," *Nature*, vol. 334, pp. 67–69, 1988.
[41] K. Nakatani and K.-W. Yau, "Calcium and light adaptation in retinal rods and cones," *Nature*, vol. 334, pp. 69–71, 1988.
[42] S. T. McCarthy, J. P. Younger, and W. G. Owen, "Free calcium concentrations in bullfrog rods determined in the presence of multiple forms of Fura-2," *Biophys. J.*, vol. 67, pp. 2076–2089, 1994.
[43] M. P. Gray-Keller and P. B. Detwiler, "The calcium feedback signal in the phototransduction cascade of vertebrate rods," *Neuron*, vol. 13, pp. 849–861, 1994.
[44] J. P. Younger, S. T. McCarthy, and W. G. Owen, "Light-dependent control of calcium in intact rods of the bullfrog *Rana catesbeiana*," *J. Neurophysiol.*, vol. 75, pp. 354–366, 1996.
[45] S. T. McCarthy, J. P. Younger, and W. G. Owen, "Dynamic, spatially nonuniform calcium regulation in frog rods exposed to light," *J. Neurophysiol.*, vol. 76, pp. 1991–2004, 1996.

Gabriel A. Silva received the B.S. degree in human physiology and biophysics and the M.S. degree in neuroscience from the University of Toronto, Toronto, ON, Canada, in 1996 and 1997, respectively. He received the Ph.D. degree in bioengineering from the University of Illinois at Chicago in 2001.

He did a postdoctoral research fellowship in nanotechnology applied to clinical neurosciences at Northwestern University (2001–2003) and is currently an Assistant Professor in the Departments of Bioengineering and Ophthalmology at the University of California at San Diego, La Jolla. His current research interests focus on the application of nanoengineering to neuroscience and, in particular, on technology-cellular interfaces and regeneration of the central nervous system following neurotrauma and degenerative disorders.

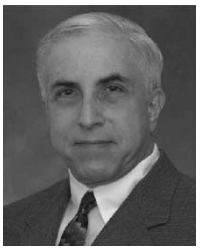

David R. Pepperberg received the B.S. degree in physics and the Ph.D. degree in biophysics from the Massachusetts Institute of Technology, Cambridge, in 1966 and 1973, respectively.

Following postdoctoral work at Harvard University, Cambridge, MA, he was Assistant Professor of Biological Sciences at Purdue University, West Lafayette, IN, from 1977 to 1983. In 1983, he moved to the Department of Ophthalmology and Visual Sciences at the University of Illinois at Chicago, where he is now Searls-Schenk Professor. His research is aimed at determining mechanisms of light and dark adaptation in retinal photoreceptors. A further focus of his recent work is the development of nanoscale structures that can interact with postsynaptic membrane receptors in diseased retina and other nerve tissue.